

About the influence of heat conductivity on the mechanical behavior of poly-crystalline shape memory alloys

Philipp Junker and Klaus Hackl*

Lehrstuhl für Allgemeine Mechanik, Ruhr-Universität Bochum, 44780 Bochum, Germany.

Abstract

Outgoing from energy conservation and the second law of thermodynamics we derive a thermo-mechanically coupled model for shape memory alloys. Additionally, we introduce a field function which allows for the modification of the dissipation coefficient. All together, the model is capable to display the localized phase transformation as well as temperature distribution which were observed in experiments.

This paper focuses on the influence of heat conductivity on numerical results for poly-crystalline shape memory alloys. The heat conductivity is identified in the approach for the entropy production. Slight changes of the entropy production ansatz yield interesting numerical results, capable of displaying experimental observations.

Key words: Shape memory alloys, Thermo-mechanically coupled model, Finite Elements, Heat conductivity

1. Introduction

The atoms in shape memory alloys may be arranged in different stable lattice structures, depending on temperature and load. These structures are well-known and denoted as *austenite* and *martensite*. At high temperatures the atoms are composed in a cubic arrangement which is called austenite. At low temperatures the material favors a less symmetric structure which can be converted from the austenite via shear and shuffle. Thus, there exists no unique transformation which maps the austenite to the sheared and shuffled state, but several which are coupled by symmetry relations. All those stable lattices are denoted by martensite whereas the variants of martensite are distinguished by means of fixed rotation matrices. From the deformation of the cubic austenitic lattice to the sheared and shuffled one of a particular martensitic variant a so-called transformation strain may be measured which serves as mechanical characterization.

Pseudo-elastic shape memory alloys are characterized by a fully reversible austenite \leftrightarrow martensite phase transformation. That means starting from a purely austenitic specimen phase transformations evolve until a combination of different martensite variants is observed. During the process of phase transition a plateau in the stress-strain diagram indicates the change of internal state. The phase transformation has a dissipative character. Energy applied to the system via a prescribed displacement and the corresponding force is not only invested in phase transitions but also in heat. Hence, releasing the specimen results in a back-transformation, but with lower force. So, a hysteresis is observed.

Many models already exist capable of describing shape-memory alloys from different viewpoints. Phenomenological models were presented e.g. in Bouvet et al. (1987), Helm and Haupt (2003) and LExcellent and Vivel

*Corresponding author. Email: philipp.junker@rub.de

(2002). In contrast to those we intend to describe phase transformations from the micromechanical side to overcome the need to find many model parameters. Other micromechanical models for poly-crystals than ours may be found in Govindjee and Miehe (2001), Stupkiewicz and Petryk (2002) and Stein and Sagar (2008). Different finite element implementations of models were presented in Pan et al. (2007). As far to our knowledge there exist no other model which is able to simultaneously describe phase transformation, localization and thermal coupling than ours.

A poly-crystal is a conglomerate of single crystals (grains) each having a different orientation. Depending on the direction of loads and the orientation of atoms a different material response may be expected. Therefore, in a poly-crystal there will always be crystals which are more favored to undergo phase transformations due to their orientation and some which will transform only slightly. In order to capture this property we use the relaxed free energy for poly-crystalline shape memory alloys introduced in Hackl and Heinen (2008). We consider a material behavior free of re-crystallization which means that the orientation of grains does not change.

The aforementioned approach for the energy is taken to derive evolution equations for the crystalline phases and a heat conduction equation by means of maximization of the entropy production for which we make an appropriate ansatz. This approach allows us to take the coupling between phase transformation and heat into account. Introducing a field function for regularization similar to Dimitrijevic and Hackl (2008) allows a modification of a dissipation coefficient in a way that the *nucleation* of martensite costs more energy as compared to its *evolution*. The impact of this modification is the formation of moving transformation fronts similar to localized plastic strains (Lüders bands) in our numerical results which coincides with experimental observations of tension tests Schaefer and Wagner (2009). The complete approach results in a remarkable improvement of our results since the original model, derived in Hackl and Heinen (2008), gives a homogeneous transformation, Junker and Hackl (2009). The regularization is necessary since the modification of the dissipation results in a loss of ellipticity and consequently in mesh dependent finite element calculations.

In the experiments the shape of those transformation fronts is changing: the inclination angle differs from specimen to specimen and a “reorientation” is observed during its movement. Transformation fronts perpendicular to the longitudinal axes of a specimen in a tension test occur as well as inclined fronts with a certain angle. One reason for this phenomenon is considered to be the thermo-mechanical coupling of the occurring phase transformations. In this paper we want to analyze the influence of the assumed ansatz on the entropy production. Since the dissipation coefficient for the heat flux may be identified as connected to heat conductivity, we present examples for different coefficients. The numerical results are brought into comparison and discussed.

2. Material Model

From thermodynamics we know that the total energy of a system is conserved. This property may be expressed by the well-known equation of energy conservation, Holzapfel (2000),

$$\dot{\Psi} + \dot{\eta}\theta + \eta\dot{\theta} = \boldsymbol{\sigma} : \dot{\boldsymbol{\varepsilon}} + h - \nabla \cdot \mathbf{q} . \quad (1)$$

In (1) Ψ denotes the specific Helmholtz free energy and η entropy, θ temperature, $\boldsymbol{\sigma}$ stress, $\boldsymbol{\varepsilon}$ strain, h internal energy wells and \mathbf{q} heat flux. Furthermore, the second law of thermodynamics has to hold which is taken here as

$$\Delta = \dot{\eta} - \frac{h}{\theta} + \nabla \cdot \left(\frac{\mathbf{q}}{\theta} \right) \geq 0 , \quad (2)$$

where Δ is the irreversible entropy production. Combination of (1) and (2) by eliminating h gives the identity

$$\Delta = \frac{1}{\theta} \left(\boldsymbol{\sigma} : \dot{\boldsymbol{\varepsilon}} - \dot{\Psi} - \eta\dot{\theta} \right) + \mathbf{q} \cdot \nabla \frac{1}{\theta} , \quad (3)$$

which has to hold at every point in time.

We know that Δ is a function of the thermodynamical fluxes of the system under consideration and we have to make an assumption on this dependence. We follow Onsager (1931) and Hackl and Fischer (2008) and maximize the entropy production Δ with respect to the thermodynamical fluxes in order to receive evolution equations. This approach is called *maximization of the dissipation* and gives for many cases same results as the *minimization*

of a dissipation potential (see Hackl and Fischer (2008)) which was used for example in Ziegler (1962), Svoboda et al. (2002) and Svoboda et al. (2006). This general approach was introduced for the thermodynamically coupled case in Hackl et al. (2010). The maximization has to be carried out under several constraints. First, the identity (3) has to be fulfilled. Additionally, the phases may only evolve under the constraint of mass conservation and positivity. The mass conservation has to be achieved in every single grain. This may be brought to formulas via the introduction of volume fractions λ_i^j . The index j belongs to grains which are described by a randomly chosen rotation matrix \mathbf{R}^j . N denotes the maximum number of grain orientations assumed ($j \in \{1, \dots, N\}$). The different phases may be distinguished via the index i whereas $i = 0$ indicates austenite and $i > 0$ the corresponding martensitic phase ($i \in \{0, \dots, n\}$, n is the number of martensite variants). Then, mass conservation reads

$$\sum_{i=0}^n \dot{\lambda}_i^j = 0 \quad \forall j. \quad (4)$$

Since negative volume fractions do not make any physical sense, we demand

$$\lambda_i^j \geq 0 \quad \forall i, j. \quad (5)$$

We introduce the Lagrangian for our problem as

$$\mathcal{L} = \Delta + \beta \left\{ \Delta - \frac{1}{\theta} \left(\boldsymbol{\sigma} : \dot{\boldsymbol{\varepsilon}} - \dot{\Psi} - \eta \dot{\theta} \right) - \mathbf{q} \cdot \nabla \frac{1}{\theta} \right\} + \sum_{j=1}^N \kappa^j \sum_{i=0}^n \dot{\lambda}_i^j - \sum_{j=1}^N \sum_{i=0}^n \gamma_i^j \dot{\lambda}_i^j \rightarrow \max_{\dot{\boldsymbol{\varepsilon}}, \dot{\boldsymbol{\lambda}}, \dot{\theta}, \mathbf{q}}, \quad (6)$$

with Lagrange parameters β and κ^j for the constraints (3) and (4) and Kuhn-Tucker parameters γ_i^j for (5), respectively. The Kuhn-Tucker parameters are only active if the constraint of positivity is not fulfilled. Thus,

$$\gamma_i^j = \begin{cases} = 0 & \text{for } \lambda_i^j > 0 \vee \left(\lambda_i^j = 0 \wedge \dot{\lambda}_i^j > 0 \right) \\ > 0 & \text{else} \end{cases}. \quad (7)$$

The Lagrangian \mathcal{L} has to be maximized with respect to its free variables, which are the rates of strain, volume fraction and temperature and the heat flux. Finding the stationary values of \mathcal{L} gives

$$\frac{\partial \mathcal{L}}{\partial \dot{\boldsymbol{\varepsilon}}} = \mathbf{0} \quad \Leftrightarrow \quad \boldsymbol{\sigma} = \frac{\partial \Psi}{\partial \boldsymbol{\varepsilon}}, \quad (8)$$

$$\frac{\partial \mathcal{L}}{\partial \dot{\boldsymbol{\lambda}}} = \mathbf{0} \quad \Leftrightarrow \quad (1 + \beta) \frac{\partial \Delta}{\partial \dot{\boldsymbol{\lambda}}} + \frac{\beta}{\theta} \frac{\partial \Psi}{\partial \dot{\boldsymbol{\lambda}}} + \boldsymbol{\kappa} - \boldsymbol{\gamma} = \mathbf{0}, \quad (9)$$

$$\frac{\partial \mathcal{L}}{\partial \dot{\theta}} = 0 \quad \Leftrightarrow \quad \eta = -\frac{\partial \Psi}{\partial \theta}, \quad (10)$$

$$\frac{\partial \mathcal{L}}{\partial \mathbf{q}} = \mathbf{0} \quad \Leftrightarrow \quad (1 + \beta) \frac{\partial \Delta}{\partial \mathbf{q}} - \beta \nabla \frac{1}{\theta} = \mathbf{0}, \quad (11)$$

with

$$\boldsymbol{\kappa} = \kappa^j \mathbf{e}_i \mathbf{e}_j, \quad \boldsymbol{\gamma} = \gamma_i^j \mathbf{e}_i \mathbf{e}_j, \quad \mathbf{e}_k : \text{unit vectors}. \quad (12)$$

This approach of maximizing the entropy production yields the constitutive equations both for stress (8) and entropy (10). The equations (8) till (11) can be used to find expressions for the Lagrange parameters β and κ^j . Plugging those expressions back into the set of equations (8) and (11) we derive evolution equations for the phases

$$\begin{cases} \frac{f}{\theta} p_i^j - \frac{f}{\theta} \frac{1}{n_{\mathcal{A}^j}} \sum_{k \in \mathcal{A}^j} p_k^j = \frac{\partial \Delta}{\partial \dot{\lambda}_i^j}, & i \in \mathcal{A}^j \\ \frac{f}{\theta} p_i^j - \frac{f}{\theta} \frac{1}{n_{\mathcal{A}^j}} \sum_{k \in \mathcal{A}^j} p_k^j = -\frac{1}{1 + \beta} \gamma_i^j, & i \notin \mathcal{A}^j \end{cases}, \quad (13)$$

where we applied the active set strategy. The active set collects all phases in each grain which fulfill the constraint of positivity (5) identically. Thus,

$$\mathcal{B}^j = \{i | \lambda_i^j = 0\} \quad (14)$$

$$\mathcal{A}^j = \{i \in \mathcal{B}^j | \dot{\lambda}_i^j > 0\} \cup \{i \notin \mathcal{B}^j\}. \quad (15)$$

In Eq. (13) $p_i^j := -\partial\Psi/\partial\lambda_i^j$ denote the thermo-mechanically conjugated driving forces, $n_{\mathcal{A}^j}$ the number of active variants in each grain j and

$$f := \frac{\beta}{1 + \beta}. \quad (16)$$

We have to make ansatzes for the energy and the entropy production. For the energy we take the approach of Hackl and Heinen (2008) in combination with Huo and Müller (1993) which is

$$\Psi^{\text{tot}} = \frac{1}{2} (\boldsymbol{\varepsilon} - \boldsymbol{\eta}_{\text{eff}}) : \mathbb{C}_{\text{eff}} : (\boldsymbol{\varepsilon} - \boldsymbol{\eta}_{\text{eff}}) + c_{\text{eff}}(\theta) \quad (17)$$

with

$$\boldsymbol{\eta}_{\text{eff}} = \sum_{j=1}^N \sum_{i=0}^n \frac{1}{N} \lambda_i^j \underbrace{(\mathbf{R}^j)^T \cdot \boldsymbol{\eta}_i \cdot \mathbf{R}^j}_{=: \boldsymbol{\eta}_i^j}, \quad \mathbb{C}_{\text{eff}} = \left[\sum_{j=1}^N \sum_{i=0}^n \frac{1}{N} \lambda_i^j (\mathbb{C}_i^j)^{-1} \right]^{-1}, \quad c_{\text{eff}}(\theta) = \sum_{j=1}^N \sum_{i=0}^n \frac{1}{N} \lambda_i^j c_i(\theta), \quad (18)$$

where $\boldsymbol{\eta}_i$, \mathbb{C}_i and c_i are the transformation strains, elastic constants and the temperature dependent chemical energy for each phase i . This energy is the result of a complete convexification of the entire energy of the system which can be expressed by the weighted sum of energies in all grains and all phases. By means of the randomly chosen rotation matrices \mathbf{R}^j we can calculate the rotated elastic constants according to

$$\mathbb{C}_{i p q r s}^j = R_{tp}^j R_{uq}^j R_{vr}^j R_{ws}^j \mathbb{C}_{i t u v w}. \quad (19)$$

For the chemical energy part we follow Huo and Müller (1993) by

$$c_i(\theta) = c_\theta (\theta - \theta_R) - c_\theta \theta \ln \left(\frac{\theta}{\theta_R} \right) + a_i - b_i \theta, \quad (20)$$

where θ_R denotes the reference temperature, c_θ the specific heat (= heat capacity) and a_i and b_i phase dependent energetic and entropic constants, respectively. Finally we use (10) and our assumption for the energy which gives the rate of entropy as

$$\dot{\eta} = c_\theta \frac{\dot{\theta}}{\theta} + \sum_{j=1}^N \sum_{i=0}^n \frac{1}{N} \dot{\lambda}_i^j b_i. \quad (21)$$

Plugging this back into (1) and introducing our ansatz for the entropy production

$$\Delta = r (|\boldsymbol{\lambda}_0|) |\dot{\boldsymbol{\lambda}}|_{\boldsymbol{\xi}} + \frac{\alpha_\theta}{2} |\mathbf{q}|^2. \quad (22)$$

($r (|\boldsymbol{\lambda}_0|)$ and α_θ are dissipation coefficients for phase transformation and heat flux, respectively) where

$$|\dot{\boldsymbol{\lambda}}|_{\boldsymbol{\xi}} = \sqrt{\sum_{j=1}^N \frac{1}{N} \sum_{i=0}^n (\dot{\lambda}_i^j)^2}, \quad (23)$$

we receive the evolution law for the phases and the heat conduction equation as

$$\dot{\lambda}_i^j = \frac{\rho}{N} \frac{f}{\theta} \left[\text{dev}_{\mathcal{A}^j} p_i^j \right]_{\mathcal{A}^j} \quad (24)$$

$$c_\theta \dot{\theta} = \mathbf{p} : \dot{\boldsymbol{\lambda}} - \nabla \cdot \left(\frac{f}{\alpha_\theta} \nabla \frac{1}{\theta} \right) - \theta \sum_{j=1}^N \sum_{i=0}^n \frac{1}{N} \dot{\lambda}_i^j b_i, \quad (25)$$

with the Kuhn-Tucker conditions

$$\rho \geq 0, \quad \phi \leq 0, \quad \rho \phi = 0 \quad (26)$$

and the consistency condition

$$\text{dev}_{\mathcal{A}^j} p_i^j \leq 0 \quad \text{for } i \in \mathcal{A}^j. \quad (27)$$

In (27), $\text{dev}_{\mathcal{A}^j} p_i^j := p_i^j - \sum_{k \in \mathcal{A}^j} p_k^j$ is called *active deviator*, $\phi = 1/N (f/\theta \text{dev}_{\mathcal{A}^j} p)^2 - r^2 (|\boldsymbol{\lambda}_0|)$ a yield function and ρ a consistency parameter determined by the constraint $\phi \leq 0$.

The argument in the function of the dissipation coefficient r is the average amount of austenite at each material point, calculated by

$$|\boldsymbol{\lambda}_0| = \sum_{j=1}^N \frac{1}{N} \lambda_0^j. \quad (28)$$

This strategy allows us to account for different energy cost regarding the *nucleation* and the *evolution* of martensite by making an appropriate ansatz for r .

3. Finite Element Implementation

The material model presented in Section 2 holds on the material point level. As usual, this model can be applied to whole samples by introducing the elastic potential. This potential Π has to achieve a minimum. The consequential minimization conditions are then used to find the displacement field under some boundary conditions. The displacements cause strains which serve as input data for the material model whereas the internal state, which is described by the volume fractions, has an influence on the stiffness and hence back on the displacements. The system of equations has to be solved in an iterative way due to its non-linearity.

The potential we use is the very common potential

$$\Pi = \int_V \Psi \, dV - \int_V \mathbf{u} \cdot (\rho \mathbf{f}) \, dV - \int_{\partial V} \mathbf{u} \cdot \mathbf{t} \, dA \quad (29)$$

which consists of the total free energy and terms due to internal and external loads (\mathbf{u} : displacements, ρ : density, \mathbf{t} : tractions on the surface). It is emphasized that it is not Ψ^{tot} which we have in (29), but an extended free energy denoted by Ψ . The extended free energy is composed of the Helmholtz free energy Ψ^{tot} and additional terms which are necessary for regularization purposes. Without any regularization the non-constant dissipation coefficient would yield mesh dependent results. The strategy to circumvent that effect is to introduce

$$\Psi = \Psi^{\text{tot}} + \underbrace{\frac{\beta_\varphi}{2} (\varphi + 1 - |\boldsymbol{\lambda}_0|)^2}_{\text{coupling}} + \underbrace{\frac{c_\varphi}{2} |\nabla \varphi|^2}_{\text{higher order term}} \quad (30)$$

with numerical coefficients β_φ and c_φ . Penalizing the gradient of the field function φ will penalize the gradient of the internal variables due to their coupling. By this approach we adopt the idea of Dimitrijevic and Hackl (2008). Although we introduce the field function mainly due to numerical reasons (mesh independence) it still may be interpreted as a *phase* field for the averaged crystallographic variants. Then, the higher order term reflects some average interface energy. The parameter c_φ controls the penalization of the interface energy. Thus, lower values

of c_φ lead to interfaces which are sharper pronounced whereas higher values lead to interfaces which are more diffuse. In the results presented below we chose $c_\varphi = 0.1$. The numerical factor β_φ may be chosen arbitrarily since it hasn't any noticeable influence on the results as shown in Dimitrijevic and Hackl (2008). From (30) we can calculate the driving forces for the volume fractions as

$$p_i^j = -\frac{\partial}{\partial \lambda_i^j} \Psi(\boldsymbol{\varepsilon}, \boldsymbol{\lambda}, |\boldsymbol{\lambda}_0|, \varphi) \quad (31)$$

$$= \frac{1}{N} \left[\boldsymbol{\eta}_i^j : \mathbb{C}_{\text{eff}} : (\boldsymbol{\varepsilon} - \boldsymbol{\eta}_{\text{eff}}) + \frac{1}{2} (\boldsymbol{\varepsilon} - \boldsymbol{\eta}_{\text{eff}}) : \left(\mathbb{C}_{\text{eff}} : \left(\mathbb{C}_i^j \right)^{-1} : \mathbb{C}_{\text{eff}} \right) : (\boldsymbol{\varepsilon} - \boldsymbol{\eta}_{\text{eff}}) - c_i(\theta) \right] \quad (32)$$

$$+ \underbrace{\xi^j \beta_\varphi (\varphi + 1 - |\boldsymbol{\lambda}_0|)}_{\star} \quad (33)$$

with additional parts (\star) due to regularization. The stationary conditions of (29) are

$$\int_V \delta \boldsymbol{\varepsilon} : \frac{\partial \Psi}{\partial \boldsymbol{\varepsilon}} dV - \int_V \delta \mathbf{u} \cdot (\rho \mathbf{f}) dV - \int_{\partial V} \delta \mathbf{u} \cdot \mathbf{t} dA = 0 \quad \forall \delta \mathbf{u} \quad (34)$$

$$\int_V \beta_\varphi (\varphi + 1 - |\boldsymbol{\lambda}_0|) \delta \varphi dV + \int_V c_\varphi \nabla \varphi \cdot \nabla \delta \varphi dV = 0 \quad \forall \delta \varphi, \quad (35)$$

which are solved by the finite element method. Additionally, we write the heat conduction equations in their variational form

$$\begin{aligned} \int_V c_\theta \dot{\theta} \delta \theta dV = \int_V \mathbf{p} : \dot{\boldsymbol{\lambda}} \delta \theta dV - \int_{\partial V} \underbrace{\frac{f}{\alpha_\theta} \nabla \frac{1}{\theta}}_{=\mathbf{q}} \cdot \mathbf{n} \delta \theta dA + \frac{1}{\alpha_\theta} \int_V f \nabla \frac{1}{\theta} \cdot \nabla \delta \theta dV \\ - \int_V \theta \sum_{j=1}^N \sum_{i=0}^n \frac{1}{N} \dot{\lambda}_i^j b_i \delta \theta dV \quad \forall \delta \theta \end{aligned} \quad (36)$$

for which we apply finite elements, too.

4. Numerical results

We present numerical results for a tensile test for pseudo-elastic Nickel Titanium. The corresponding transformation strains as well as the elastic constants are collected according to Wagner and Windl (2008) in Tab. 1 and 2, respectively. In all cases the boundary conditions remain the same: for both sides we prescribe the displacements of all first two rows of nodes inside the discretization, i.e. the boundary nodes are excluded. On the left hand side all displacements are zero, whereas the displacements at the right hand side are prescribed in longitudinal direction. Through these boundary conditions the experimental conditions can be simulated best. The dimensions of the specimen are 35 mm, 3.3 mm and 0.68 mm (length, height, depth).

Although the rotation matrices are chosen randomly, we receive reproducible results since we calculate with a relatively high number of grains, exactly $N = 100$.

The plot of the assumed chemical energies for austenite and all variants of martensite is shown in Fig. (1) (left) as well as the plot of the dissipation coefficient as function of the average amount of austenite (right).

The functions for the chemical energies are

$$c_0(\theta) = 0.01(\theta - 293.15) - 0.01 \theta \ln \frac{\theta}{293.15} + 2.61 - 0.0089 \theta \quad [\text{MPa}], \quad (37)$$

$$c_{i \geq 0}(\theta) = 0.01(\theta - 293.15) - 0.01 \theta \ln \frac{\theta}{293.15} + 1.76 - 0.0060 \theta \quad [\text{MPa}]. \quad (38)$$

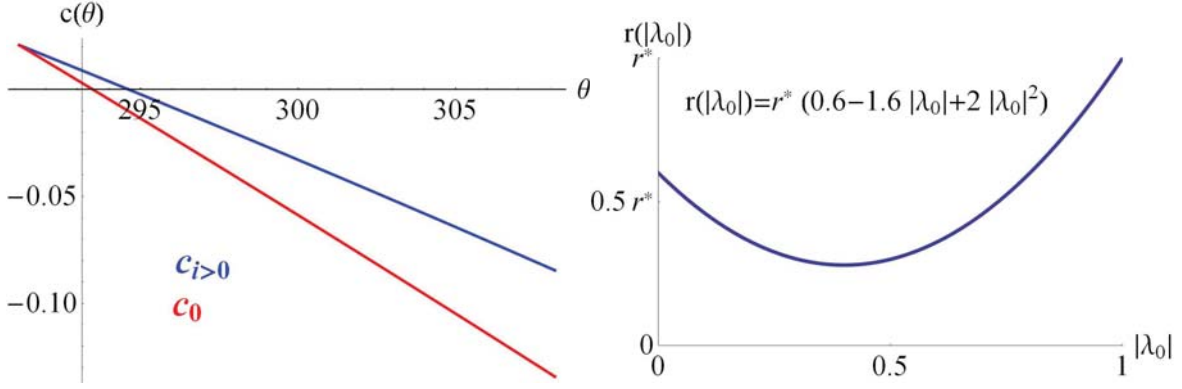


Figure 1: Left: chemical energies for austenite c_0 and all martensite variants $c_{i>0}$. Right: assumed function for the dissipation coefficient $r(|\lambda_0|)$.

The dissipation coefficient r is determined by the constraint that *nucleation* of martensite (r_{start}) costs more energy than its *evolution* (r_{av}). Furthermore, the completion of the transformation of austenite (r_{finish}) will again dissipate more energy as compared to the “average evolution” of martensite, due to the highly increasing number of interfaces (between austenite and martensite and between martensite and martensite). However, less energy is dissipated as compared to the case when the very first nucleation of martensitic grains takes place. The translation of these physical assumptions into a mathematical scheme is done via

$$r_{\text{start}} = r(1) \quad (39)$$

$$r_{\text{finish}} = r(0) \quad (40)$$

$$r_{\text{av}} = \int_0^1 r(|\lambda_0|) d|\lambda_0| \quad (41)$$

$$r_{\text{av}} < r_{\text{finish}} < r_{\text{start}} . \quad (42)$$

For the different dissipation coefficients we assume

$$r_{\text{start}} = r^* , \quad r_{\text{finish}} = \frac{3}{5}r^* \quad r_{\text{av}} = \frac{7}{15}r^* , \quad (43)$$

with $r^* = 0.018$ MPa/K. By quadratic interpolation this yields

$$r(|\lambda_0|) = 0.018 \cdot (0.6 - 1.6|\lambda_0| + 2|\lambda_0|^2) \quad [\text{MPa/K}] . \quad (44)$$

We mention that the exact values for r_{start} , r_{finish} and r_{av} are not essential since a variation gives similar results.

In the following we present different numerical results for the same boundary value problem described above. The only parameter we change is the value for the dissipation coefficient for the heat flux α_θ from Eq. (22), namely $\alpha_\theta = \{1.0, 2.5, 5.0\} \cdot 10^{-3}$ mmK/W.

In Fig. (2) we present the distribution of austenite at various steps in time for $\alpha_\theta = 1.0 \cdot 10^{-3}$ mmK/W. In this case the phase transformation initializes where the specimen is “clamped” (where the displacements are prescribed). Due to the released heat the increased temperature causes the material to evolve a further transformation zone. The relatively small value of α_θ results in a homogeneous temperature conduction so that in the center of the specimen the further front is created. Any small deviation of the front’s orientation at the ends from being perpendicular to the longitudinal axes is damped out (the randomness of the orientation matrices yields very small stochastic variations). During further loading phase transformations can be observed in all three zones.

The corresponding distribution of temperature can be seen in Fig. (3). We present the temperature distribution for some selected points in time. It can be seen that the phase transformation serves as internal heat source

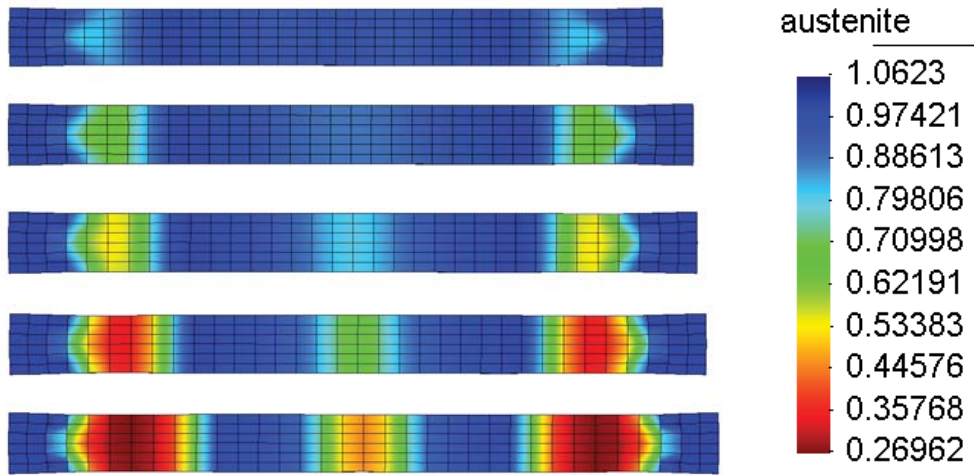


Figure 2: Distribution of the austenite phase over the specimen at different load steps, $\alpha_\theta = 1.0 \cdot 10^{-3}$ mmK/W.

since energy is dissipated during transition. During the increasing prescribed displacements the heat sources move through the specimen analogously to the transformation fronts.

In contrast to Fig. (2) we see a different behavior in Fig. (4). Here, we changed the dissipation coefficient slightly to $\alpha_\theta = 2.5 \cdot 10^{-3}$ mmK/W. However, the general material response in the beginning is similar. The transformation starts where stress peaks occur but almost simultaneously at two points in the specimen phase transitions initialize. Due to some inclination of the initial fronts the temperature field is not perpendicular either and caused by the a slower heat transport the additional phase transformation happens more closely to the ends. All the fronts proceed localized in a front like manner after their formation. Interestingly, the additional fronts are not perpendicular to the longitudinal axes anymore as they are in the previous case. Due to the changed heat conduction, the austenitic state is more stable in some areas and less stable in others. This influence results in a non-perpendicular but inclined direction in which the transformation spreads over the cross section.

The temperature distribution which corresponds to the second example is presented in Fig. 5. Since the temperature flows through the specimen its distribution is not as localized as the distribution of phases and the non-perpendicular front is smeared out. Again, the temperature sources move through the specimen.

The last example presented in this paper is based on a dissipation parameter for the heat flux of $\alpha_\theta = 5.0 \cdot 10^{-3}$ mmK/W. The resulting distribution of the austenitic phase is shown in Fig. 6. We recognize that again at the ends the initial phase transformation occurs. Here, the heat conductivity is the smallest one. Therefore the heat produced during the phase transformation at the ends of the specimen is not transported to the center very fast but remains mostly in the area of its release. Again, as in all examples here, the produced heat is high enough to stabilize the austenite in a remarkable way. Hence, again more zones of phase transformation occur, in this example quite close to the ends, similar as in the previous example. But in contrast to this one, any inclination of the initial zones does not affect the further developed zones since the "transporting variable", the temperature distribution, moves too slow according to the low heat conductivity. The impact of this fact is that the zones evolve perpendicular to the longitudinal axes of the specimen, similar as the first example, but now with two additional zones instead of only one. In Fig. 7 the temperature distribution for some points in time is shown. It can be seen that obviously in the regions where the phase transformation has initialized the temperature is the highest.

Another interesting point is the global mechanical response of the specimen. This behavior can be captured in force displacement diagrams which we present in Fig. 8. It is obvious that all specimens react in a very similar way during the elastic regime. First when the phase transformations take place some slight differences can be

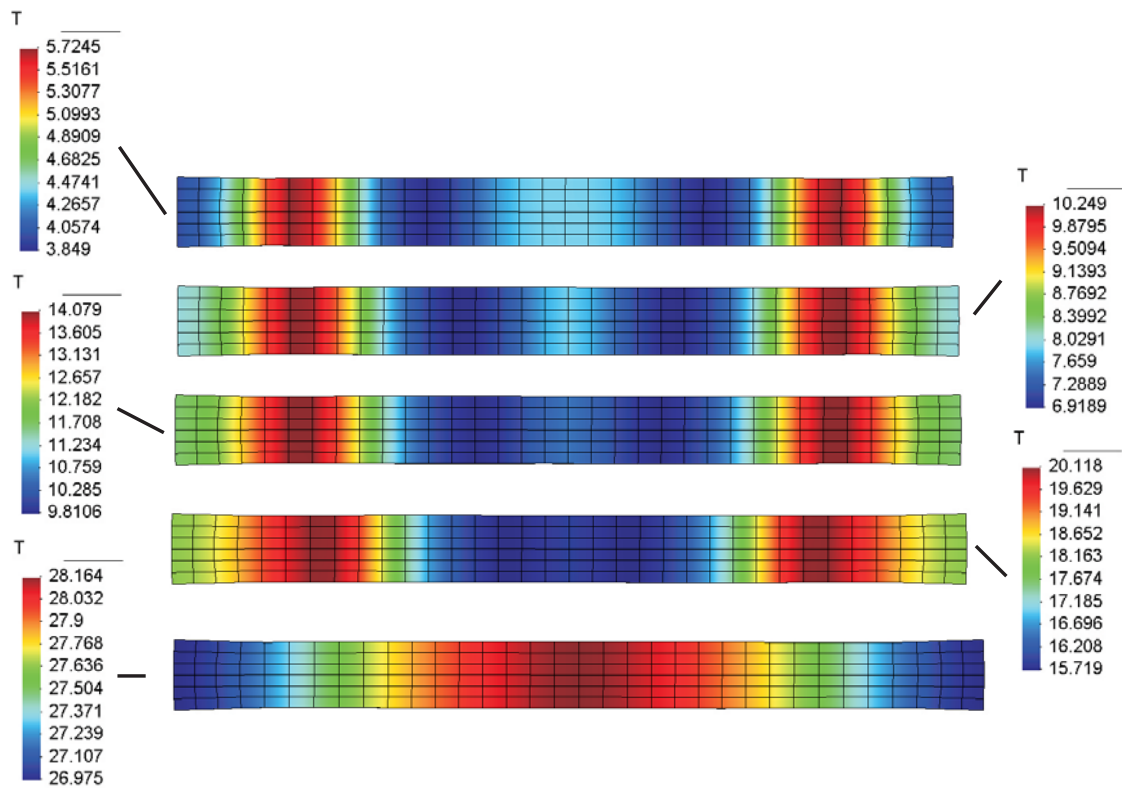


Figure 3: Distribution of the temperature over the specimen at different load steps with according legends, $\alpha_\theta = 1.0 \cdot 10^{-3}$ mmK/W.

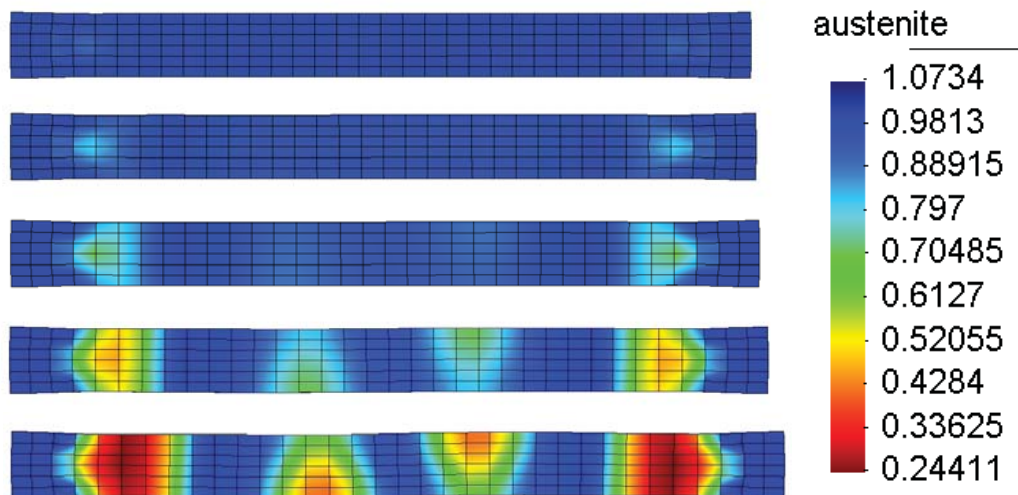


Figure 4: Distribution of the austenite phase over the specimen at different load steps, $\alpha_\theta = 2.5 \cdot 10^{-3}$ mmK/W.

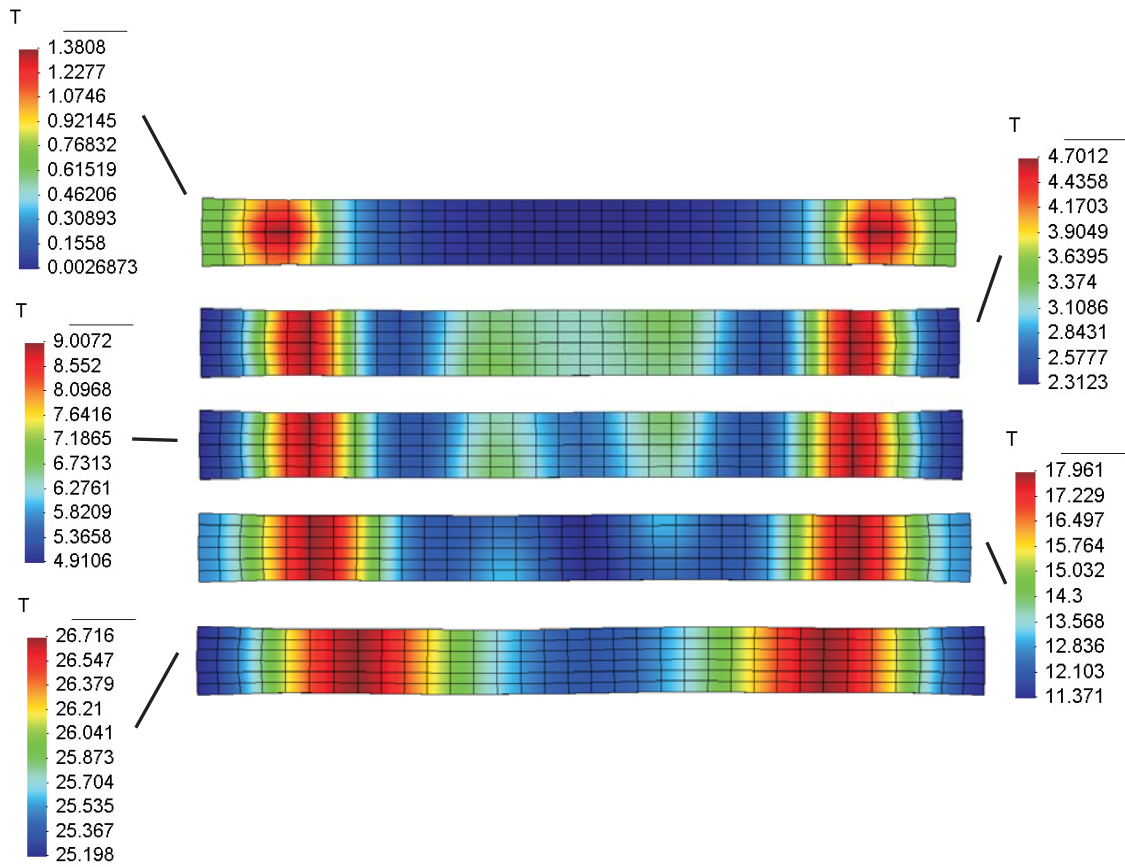


Figure 5: Distribution of the temperature over the specimen at different load steps with according legends, $\alpha_\theta = 2.5 \cdot 10^{-3}$ mmK/W.

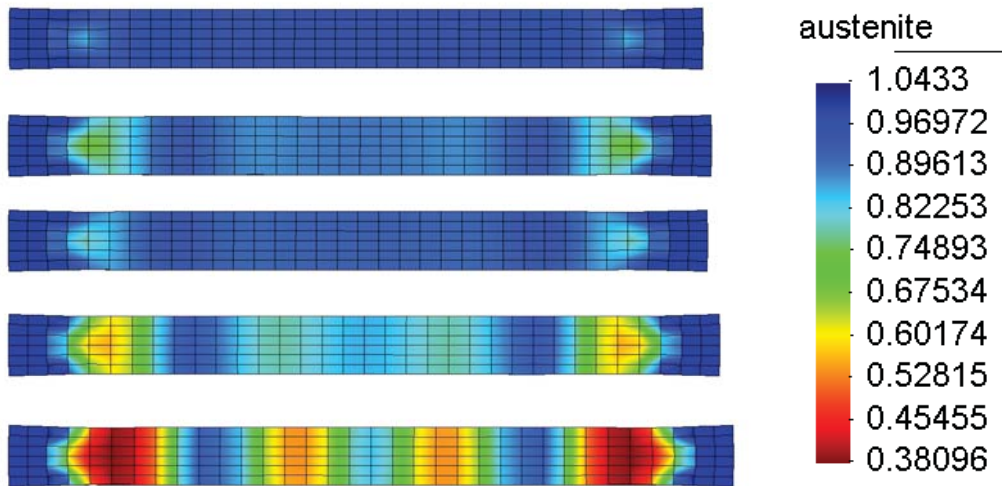


Figure 6: Distribution of the austenite phase over the specimen at different load steps, $\alpha_\theta = 5.0 \cdot 10^{-3}$ mmK/W.

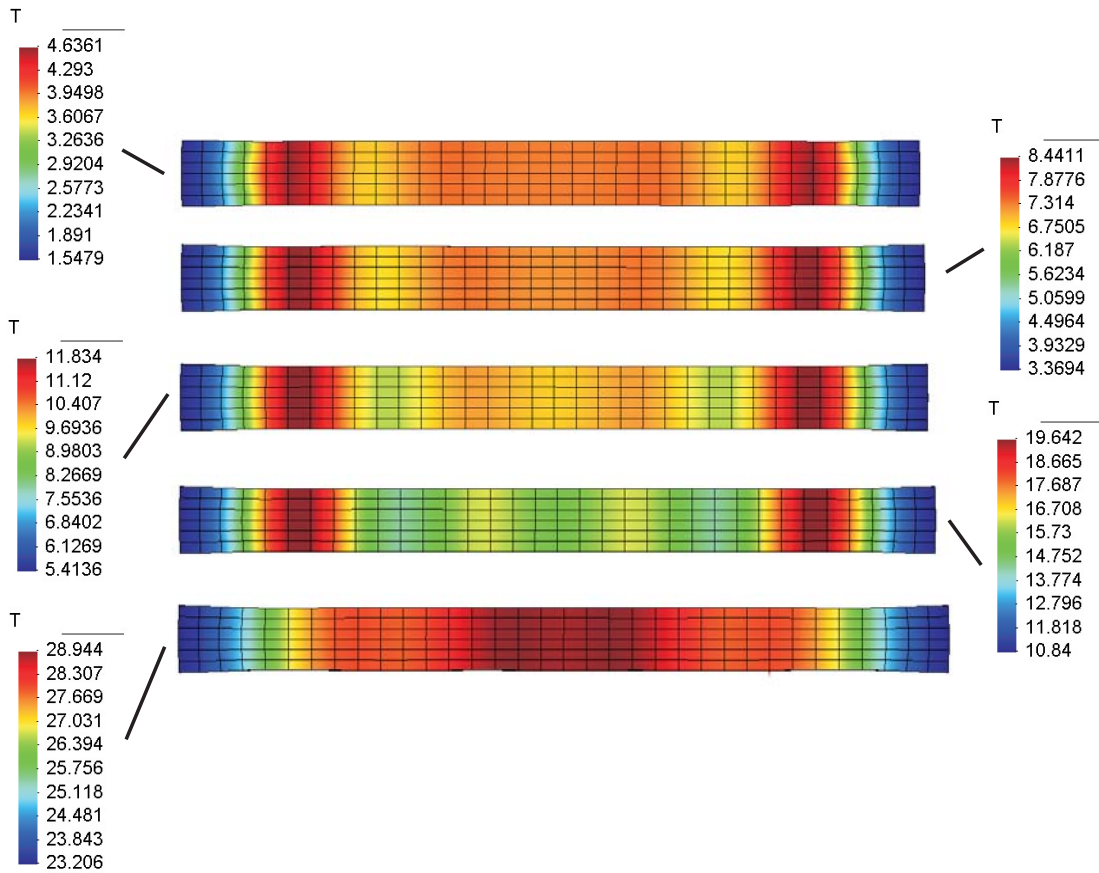


Figure 7: Distribution of the temperature over the specimen at different load steps with according legends, $\alpha_\theta = 5.0 \cdot 10^{-3}$ mmK/W.

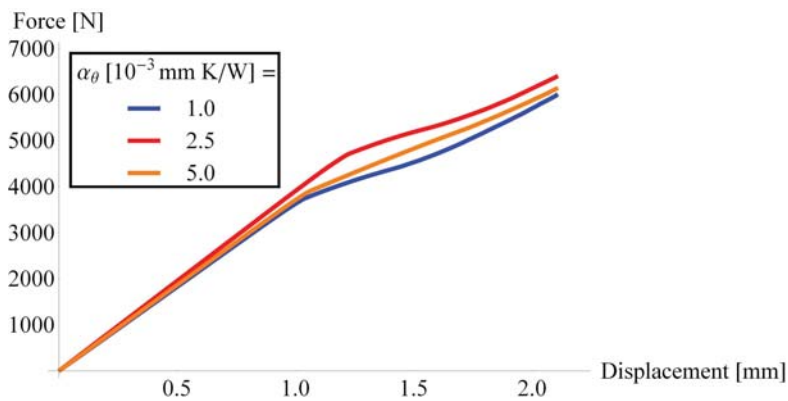


Figure 8: Force displacement diagram for the three different cases of dissipation coefficient.

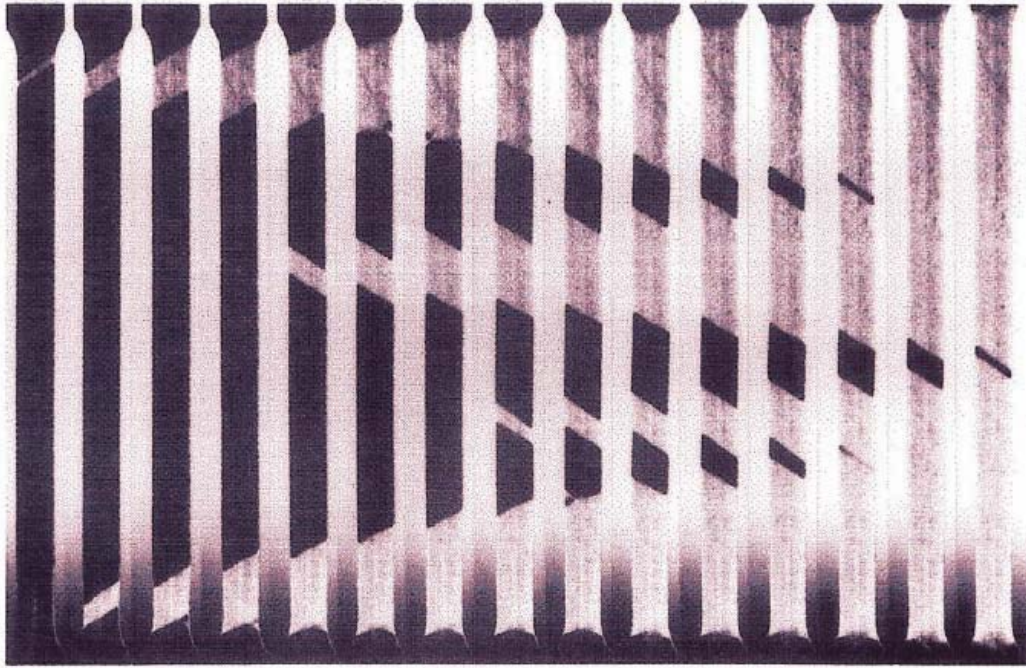


Figure 9: Experimentally measured phase distribution. Courtesy of A. Shaw.

recognized. All branches do not show a plateau during transformation which coincides well with experimental findings for tension test under high velocities, e.g. Shaw (2000). Due to temperature effects the localized transformation is less pronounced the faster the velocity is, as we have shown in our numerical results. Transformation is influenced by two opposing effects: on the one hand stress will favor the material to transform, on the other hand temperature will stabilize the austenitic phase. The interaction of both factors results in the non-linear but not plateau-like material behavior observed. The blue branch in Fig. 8 corresponds to the distribution of austenite presented first. This branch has the highest similarity to a plateau which is reasonable due to the *initial* nucleation of the two fronts and a *subsequent* formation of the middle front. The orange branch belongs to the distribution of the austenitic phase with various fronts presented last. In that case the material response is almost linear during transformation but with a different slope than in the part without phase transformations. That corresponds to the fact that due to various fronts nearly everywhere in the specimen transformations are going on, but those are slowed due to the high production of heat. The last, red branch gives the material response for the case with transformation fronts with inclined angle. Here, we have a similar material response compared to the blue branch but with higher strains and stresses. At the first glance this result may seem surprising, but since a more localized distribution and less favorable transportation of heat in the specimen is present in this case the rate of transformation is slowed down. Due to the loss effective heat conduction the stabilizing effect on the austenitic phase is more pronounced and can be identified in the global material response.

5. Conclusions

Experimental results for a tension test are presented in Shaw (2000). There, the localized strain distribution was measured (which corresponds to a change of phase). The result is recalled in Fig. 9. We see that various inclinations of the front orientations may be observed in reality, e.g. the front in the upper end is changing its orientation during loading. Since our model is capable to display this phenomenon via a change of the dissipation coefficient α_θ , one reason for the change may be a locally different heat conductivity due to inhomogeneities in the alloy composition.

We presented numerical simulations of poly-crystalline shape memory alloys based on a micro-mechanically well motivated model. The model is able to predict the localized transformation as well as the corresponding distribution of temperature and their coupling. In this paper we focused on the influence of the heat conductivity. Small changes of the dissipation coefficient cause the material to show different behavior. Due to the randomly chosen rotation matrices the initial orientation of the first transformation front always differs very slightly. Thus, the temperature distribution shows as well some "initial direction" of the fronts. Those very small deviations are then more or less pronounced depending on the heat conductivity. Coupling of the whole system evokes that the direction of the transformation front depends on *where* and *with which orientation* additional fronts evolve. The evolution of all fronts is then coupled again. This result may give a hint why a different material behavior is observed in the same test. The locally different heat conductivity in real specimens due to variation of the elementary composition of the alloy may be one reason for the observed changes in the orientation of the transformation fronts. Of course, the influence of dislocations and the current distribution of grain boundaries is not taken into account explicitly. On the other hand, those effects are always random so that we may interpret our randomly chosen orientations to reflect this point in some way.

Some future goals of ours are the implementation of locally random parameters for the dissipation coefficient and the analysis of pseudo-plastic problems via our model.

 Table 1: Transformation strains for cubic to monoclinic transforming NiTi. $\bar{\alpha} = 0.02381$, $\bar{\beta} = -0.02480$, $\bar{\delta} = 0.07528$, $\bar{\epsilon} = 0.04969$

$$\begin{array}{ccc}
 \boldsymbol{\eta}_1 = \begin{pmatrix} \bar{\alpha} & \bar{\delta} & \bar{\epsilon} \\ \bar{\delta} & \bar{\alpha} & \bar{\epsilon} \\ \bar{\epsilon} & \bar{\epsilon} & \bar{\beta} \end{pmatrix} & \boldsymbol{\eta}_2 = \begin{pmatrix} \bar{\alpha} & \bar{\delta} & -\bar{\epsilon} \\ \bar{\delta} & \bar{\alpha} & -\bar{\epsilon} \\ -\bar{\epsilon} & -\bar{\epsilon} & \bar{\beta} \end{pmatrix} & \boldsymbol{\eta}_3 = \begin{pmatrix} \bar{\alpha} & -\bar{\delta} & -\bar{\epsilon} \\ -\bar{\delta} & \bar{\alpha} & \bar{\epsilon} \\ -\bar{\epsilon} & \bar{\epsilon} & \bar{\beta} \end{pmatrix} \\
 \boldsymbol{\eta}_4 = \begin{pmatrix} \bar{\alpha} & -\bar{\delta} & \bar{\epsilon} \\ -\bar{\delta} & \bar{\alpha} & -\bar{\epsilon} \\ \bar{\epsilon} & -\bar{\epsilon} & \bar{\beta} \end{pmatrix} & \boldsymbol{\eta}_5 = \begin{pmatrix} \bar{\alpha} & \bar{\epsilon} & \bar{\delta} \\ \bar{\epsilon} & \bar{\beta} & \bar{\epsilon} \\ \bar{\delta} & \bar{\epsilon} & \bar{\alpha} \end{pmatrix} & \boldsymbol{\eta}_6 = \begin{pmatrix} \bar{\alpha} & -\bar{\epsilon} & \bar{\delta} \\ -\bar{\epsilon} & \bar{\beta} & -\bar{\epsilon} \\ \bar{\delta} & -\bar{\epsilon} & \bar{\alpha} \end{pmatrix} \\
 \boldsymbol{\eta}_7 = \begin{pmatrix} \bar{\alpha} & -\bar{\epsilon} & -\bar{\delta} \\ -\bar{\epsilon} & \bar{\beta} & \bar{\epsilon} \\ -\bar{\delta} & \bar{\epsilon} & \bar{\alpha} \end{pmatrix} & \boldsymbol{\eta}_8 = \begin{pmatrix} \bar{\alpha} & \bar{\epsilon} & -\bar{\delta} \\ \bar{\epsilon} & \bar{\beta} & -\bar{\epsilon} \\ -\bar{\delta} & -\bar{\epsilon} & \bar{\alpha} \end{pmatrix} & \boldsymbol{\eta}_9 = \begin{pmatrix} \bar{\beta} & \bar{\epsilon} & \bar{\epsilon} \\ \bar{\epsilon} & \bar{\alpha} & \bar{\delta} \\ \bar{\epsilon} & \bar{\delta} & \bar{\alpha} \end{pmatrix} \\
 \boldsymbol{\eta}_{10} = \begin{pmatrix} \bar{\beta} & -\bar{\epsilon} & -\bar{\epsilon} \\ -\bar{\epsilon} & \bar{\alpha} & \bar{\delta} \\ -\bar{\epsilon} & \bar{\delta} & \bar{\alpha} \end{pmatrix} & \boldsymbol{\eta}_{11} = \begin{pmatrix} \bar{\beta} & -\bar{\epsilon} & \bar{\epsilon} \\ -\bar{\epsilon} & \bar{\alpha} & -\bar{\delta} \\ \bar{\epsilon} & -\bar{\delta} & \bar{\alpha} \end{pmatrix} & \boldsymbol{\eta}_{12} = \begin{pmatrix} \bar{\beta} & \bar{\epsilon} & -\bar{\epsilon} \\ \bar{\epsilon} & \bar{\alpha} & -\bar{\delta} \\ -\bar{\epsilon} & -\bar{\delta} & \bar{\alpha} \end{pmatrix}
 \end{array}$$

Table 2: Elastic constants for austenite and martensite

$$\mathbb{C}_{\text{aust}} = \begin{pmatrix} 140 & 110 & 110 & 0 & 0 & 0 \\ 110 & 140 & 110 & 0 & 0 & 0 \\ 110 & 110 & 140 & 0 & 0 & 0 \\ 0 & 0 & 0 & 32 & 0 & 0 \\ 0 & 0 & 0 & 0 & 32 & 0 \\ 0 & 0 & 0 & 0 & 0 & 32 \end{pmatrix} \text{ GPa} \quad \mathbb{C}_{\text{mart}} = \begin{pmatrix} 223 & 129 & 99 & 0 & 27 & 0 \\ 129 & 241 & 125 & 0 & -9 & 0 \\ 99 & 125 & 200 & 0 & 4 & 0 \\ 0 & 0 & 0 & 76 & 0 & -4 \\ 27 & -9 & 4 & 0 & 21 & 0 \\ 0 & 0 & 0 & -4 & 0 & 77 \end{pmatrix} \text{ GPa}$$

References

- Bouvet, C., Calloch, S. and Lexcellent, C., 1987 A phenomenological model for pseudoelasticity of shape memory alloys under multiaxial proportional and nonproportional loadings, *Eur. J. Mech. A-Solids* **23**, 37–61.
- Dimitrijevic, B. and Hackl, K., 2008 A method for gradient enhancement of continuum damage models, *Tech. Mech.* **28**, 43–52.
- Govindjee, S., Miehe, C., 2001 A multi-variant martensitic phase transformation model: formulation and numerical implementation, *Comp. Meth. Appl. Mech. Engrg.* **191**, 215–238.

- Govindjee, S., Hackl, K., Heinen, R., 2003 An upper bound to the free energy of mixing by twin-compatible lamination for n-variant martensitic phase transformations, *Continuum Mech. Thermodyn.* **18**, 443–453.
- Hackl, K. and Fischer F. D., 2008 On the relation between the principle of maximum dissipation and inelastic evolution given by dissipation potentials, *Proc. R. Soc. A* **464**, 117–132.
- Hackl, K., Fischer F. D. and Svoboda, J., 2010 A study on the principle of maximum dissipation for coupled and non-coupled non-isothermal processes in materials, *Proc. R. Soc. A* received and accepted.
- Hackl, K. and Heinen, R., 2008 A micromechanical model for pretextured polycrystalline shape-memory alloys including elastic anisotropy, *Continuum Mech. Thermodyn.* **19**, 499.
- Heinen, R., Hackl, K., 2007 On the calculation of energy-minimizing phase fractions in shape memory alloys, *Comput. Meth. Appl. Mech. Eng.* **196**, 2401–2412.
- Helm, D. and Haupt, P., 2003 Shape memory behaviour: modelling within continuum thermomechanics, *Int. J. Solids Struct.* **40**, 827–849.
- Holzappel, G.A., 2000 "Nonlinear Solid Mechanics", Wiley.
- Huo, Y. and Müller, I., 1993 Nonequilibrium thermodynamics of pseudoelasticity, *Continuum Mech. Thermodyn.* **5**, 163–204.
- Junker, P. and Hackl, K., 2009 Numerical simulations of poly-crystalline shape-memory alloys based on a micromechanical model, *PAMM* **9**, 339-340.
- Lexcellent, C. and Vivet, A., 2002 Experimental and numerical determination of the initial surface of phase transformation under biaxial loading in some polycrystalline shape-memory alloys, *J. Mech. Phys. Sol.* **50**, 2717–2735.
- Mehrabadi, M.M. and Cowin, S.C., 1987 Eigentensors of linear anisotropic elastic materials, *Q. J. Mech. Appl. Math.* **43**, 15–41.
- Onsager, L., 1931 Reciprocal Relations in Irreversible Processes, *Phys. Rev.* **37**, 405–426.
- Pan, H., Thamburaja, P. and Chau, F. S., 2007 Multi-axial behavior of shape-memory alloys undergoing martensitic reorientation and detwinning, *Int. J. Plasticity* **23**, 711–732.
- Schaefer, A. and Wagner, M.F.-X., 2009 Strain mapping at propagating interfaces in pseudoelastic NiTi, *EDP Sciences ESOMAT 2009*, art. 06031.
- Shaw, J.A., 2000 Simulations of Localized Thermo-mechanical Behavior in a NiTi Shape Memory Alloy, *Int. J. Plasticity* **16**, 541–562.
- Stein, E. and Sagar, G., 2008 Theory and finite element computation of cyclic martensitic phase transformation at finite strain, *Int. J. Numer. Meth. Engng* **74**, 1–31.
- Stupkiewicz, S. and Petryk, H., 2002 Modelling of laminated micro-structures in stress-induced martensitic transformation, *J. Mech. Phys. Sol.* **50**, 2303–2331.
- Svoboda, J., Fischer, F. D., Fratzl, P. and Kroupa, A. 2002 Diffusion in multi-component systems with no or dense sources and sinks for vacancies, *Acta Mater.* **50**, 1369-1381.
- Svoboda, J., Fischer, F. D. and Fratzl, P. 2006 Diffusion and creep in multi-component alloys with non-ideal sources and sinks for vacancies, *Acta Mater.* **54**, 3043-3053.
- Wagner, M.F.-X. and Windl., W., 2008 Lattice stability, elastic constants and macroscopic moduli of NiTi martensites from first principles, *Acta Materialia* **56**, 6232-6245.
- Ziegler, H., 1962 Some extremum principles in irreversible thermodynamics with applications to continuum mechanics. In *Progress in solid mechanics* (eds I. N. Sneddon & R. Hill), pp. 92193. Amsterdam, The Netherlands: North-Holland.